Journal of Building Engineering 75 (2023) 106854

Contents lists available at ScienceDirect

Journal of Building Engineering

journal homepage: www.elsevier.com/locate/jobe

A experimental characterization of seismic plus thermal energy retrofitting techniques for masonry infill walls

André Furtado [a], Hugo Rodrigues [b,*], António Arêde [c], Humberto Varum [c]

[a] CERIS, Instituto Superior Técnico, Universidade de Lisboa, Portugal
[b] RISCO, Department of Civil Engineering, University of Aveiro, Portugal
[c] CONSTRUCT, Department of Civil Engineering, Faculty of Engineering of the University of Porto, Portugal

ARTICLE INFO

Keywords:
Masonry infill walls
Out-of-plane behaviour
Retrofitting
Seismic plus energy retrofitting
Experimental testing

ABSTRACT

The renovation and refurbishment of existing envelopes of existing RC buildings are usually performed, focusing only on improving their structural or thermal energy characteristics. However, international concern about the sustainability and resilience of existing building structures demands the rethinking of retrofitting techniques that tackle both aspects simultaneously, making the envelopes more energy efficient and seismic safer. Based on this motivation, a testing campaign was carried out to validate the efficiency of novel seismic plus energy retrofitting techniques. Five full-scale specimens were built, three of them with seismic plus energy retrofitting and two of them with solutions developed to improve each case. The five specimens were subjected to pure OOP quasi-static loadings until reached the collapse or partial collapse. The results of the retrofitted walls were compared with a reference specimen (i.e. non-retrofitted) to assess the efficiency of each solution. From the results, it was observed that the novel combined retrofitting can improve the thermal transmittance of the wall by around 70%, and the strength and deformation capacity by up to 125% and 340%, respectively.

1. Introduction

The renovation and refurbishment of the envelopes of existing Reinforced Concrete (RC) buildings are usually performed focusing only on improving their thermal characteristics. However, international concern about the sustainability and resilience of existing building structures demands the rethinking of retrofitting techniques that tackle not only the thermal efficiency but also the behaviour of other aspects simultaneously, like, for example, in seismic-prone areas making the envelopes more energy efficient and at the same time seismic safer. Recent policies promote only non-structural rehabilitation, i.e. improving the buildings' energy efficiency, aiming to improve energy efficiency and reduce carbon dioxide emissions, however, the structural characteristics of the wall will remain, thus neglecting this unique opportunity to reduce their seismic vulnerability and simultaneously also upgrading the seismic safety and resilience of the existing buildings against natural hazards, extreme events like earthquakes.

The post-earthquake damage survey assessment of several recent major events highlighted the significant vulnerability of the masonry infill walls when subjected to out-of-plane (OOP) seismic loadings [1–4]. It is reported that common construction practices and the interaction between in-plane and out-of-plane seismic loadings are responsible for the increased collapse vulnerability. De Risi et al. [5] estimated the impact of the infill walls on the repair costs of damaged RC structures to be around 50% of the total costs. One

* Corresponding author.
E-mail address: hrodrigues@ua.pt (H. Rodrigues).

https://doi.org/10.1016/j.jobe.2023.106854
Received 27 January 2023; Received in revised form 21 April 2023; Accepted 15 May 2023
Available online 4 June 2023

aspect that needs to be also taken into account is that the first energy codes were implemented only after 1970 [6], which means that the buildings constructed before 1980 may have serious deficiencies in energy performance. Also, the masonry infill walls comprise a significant fraction of a building envelope and are expected to provide thermal and acoustic comfort within a building without compromising its aesthetics. They are responsible for a significant part of the building's energy efficiency.

The majority of these structures were built before modern seismic codes. Moreover, the seismic response of some non-structural elements has been directly responsible for damages, collapses, casualties, and economic losses and the impact on post-earthquake rehabilitation costs [6] is estimated to be about 50% of the total repair costs [5]. Around 40% of the EU buildings are located in seismic regions and designed with sub-standard safety requirements, of which 65% of them need both energy and seismic retrofit. Independent seismic [7] or energy retrofitting interventions [8] are available and are usually adopted. However, a holistic approach comprising the combination of structural safety, energy efficiency, and sustainability for upgrading existing buildings is still missing.

Up to now, several studies have been performed in order to develop and validate retrofitting strategies that reduce the collapse vulnerability of walls located in the envelopes of buildings. Different techniques can be used within this strategy, namely: Fibre Reinforced Polymers (FRP), Engineered Cementitious Composites (ECC), Textile Reinforced Mortars (TRM), ferrocement and bed joints' reinforcement. Concerning the FRP, different authors reported that the technique would be effective if the proper connection of the FRP to the reinforced concrete elements is ensured [9,10]. The same was reported by authors that studied the use of ECC [11,12] and TRM to strengthen masonry infill walls [13–15]. The anchorage of the retrofitting material is key in the seismic retrofitting of infill walls. Different types of connectors are available to fix the strengthening material to the reinforced concrete elements, such as plastic connectors, L-shape glass FRP connectors, steel connectors and FRP rods. From the techniques listed above, the TRM is the cheaper one and easy to apply, which makes it a solution with a high potential for application.

Concerning the energy retrofitting, the external thermal insulation composite (ETIC) system is one of the most popular techniques [16,17]. Cement panels for façades refurbishment are also used. This type of technique is comprised of a galvanized steel or aluminum support structure attached to the supporting wall substrate, bearing a cement panel with a decorative coating. Also, thermal insulation plasters are being used but never being investigated for their contribution to the flexural strength of masonry infill walls.

Recently, the efficiency of Seismic plus Energy (SpE) retrofitting techniques to improve the seismic performance of infill walls started to be investigated. Manos et al. [18] studied the structural performance of masonry infill walls strengthened with ETICS. The retrofitted walls were subjected to flexural strength loadings. Later, Manos et al. [19] investigated the in-plane performance of the same ETIC system tested before. It was concluded that the walls with ETIC system did not collapse, even when the wall reached large OOP deformation due to plastic connectors used according to the authors. It was also reported that the presence of connectors increased the flexural capacity and prevented brittle behaviour than the as-built configuration.

Recent studies focused on testing the efficiency of combining structural plus energy retrofitting techniques. The technique selected in all the study consists of upgrading the textile-reinforced mortar with thermal insulation materials. This technique combines the textile-reinforced mortar and the thermal insulation composite system [20]. Later, Karlos et al. [21] carried out a series of medium-scale tests on masonry walls subjected to OOP cyclic loadings. The authors investigated the effect of placing the TRM in a sandwich form (over and under the insulation) or outside the insulation, one-sided or two-sided TRM jacketing. The combined TRM with thermal energy insulation scheme was revealed to be quite effective for the case of out-of-plane loading when proper bonding between the different layers is achieved. According to the experimental results, positioning the reinforcement outside the thermal insulation improved the wall strength and deformation capacity compared to TRM jacketing alone. Gkournelos et al. [22] tested 12 walls retrofitted with textile-reinforced mortar combined or not with expanded polystyrene as thermal insulation material under in-plane diagonal compression and out-of-plane bending on walls with or without prior in-plane damage. Masonry walls with both textile-reinforced mortar and thermal insulation and no prior in-plane damage reached more than 25% out-of-plane strength and 50% deformation at peak load. The validation of the SpE retrofitting is still missing for full-scale specimens and for walls built inside RC frames subjected to pure OOP loading demands. Also, the characterization of the OOP behaviour of full-scale walls retrofitted ETIC system is also missing.

Based on this motivation, a testing campaign was carried out to validate the efficiency of novel SpE retrofitting techniques against the independent ones. Five full-scale specimens were built, three of them with SpE retrofitting and two of them with independent. The independent seismic retrofitting technique was a TRM-based technique, and the energy retrofitting was an ETIC system. The five specimens were subjected to pure OOP quasi-static loadings to reach their collapse or partial collapse. Also, the results of the retrofitted walls were compared with a reference specimen (i.e. non-retrofitted) to assess the retrofit benefit better. The mechanical properties of the adopted materials are characterized and presented. The results will be presented in terms of damage evolution, OOP force-displacement responses, secant stiffness and heat transfer coefficient (Uvalue). The efficiency of each technique will be assessed through an independent approach, i.e. analysing single performance indicator and a holistic approach by combining structural/seismic and energy indicators.

2. Testing campaign

2.1. General description and objectives

Aiming to investigate the efficiency of SpE retrofitting techniques for envelopes of RC buildings it is vital to study the OOP behaviour of masonry infill walls with independent retrofitting, i.e. with only energy retrofitting and only seismic retrofitting. Three main objectives were defined for this testing campaign: i) evaluate the OOP seismic behaviour of masonry infill walls with SpE retrofitting; ii) evaluate the OOP seismic behaviour of masonry infill walls with energy retrofitting; iii) evaluate the OOP seismic behaviour of masonry infill walls with seismic retrofitting.

To accomplish this objective five full-scale OOP were performed, one of them with independent energy retrofitting (specimen E), one with independent seismic retrofitting (specimen S) and the three remaining with combined SpE retrofitting (specimens ES_1, ES2 and ES_3). The specimen E was retrofitted with the traditional External Thermal Insulation Composite System (commonly known as ETICS). This technique is quite popular in the current renovation wave of the existing building stock for RC and masonry building structures. Specimen S was retrofitted with the Textile-Reinforced Mortar (TRM) technique. Previous studies were already developed assessing the efficiency of this technique, but remain some open issues concerning the connections between the frame and the strengthening material. The approach used in the specimen S connection system was different from the ones in the literature. Concerning the specimens ES_1 and ES_2, they were retrofitted with SpE techniques. The techniques were based on the combination between TRM and ETICS, i.e. the technique used for specimen ES_1 consisted on applying first the ETICS in the external surface wall and after that, the TRM was placed over the ETICS. The approach used in specimen ES_2 was different, i.e. the TRM was first placed in the external surface of the wall. After that, the ETICS were placed over the TRM. Finally, ES_3 was retrofitted with the Reinforced Thermal Insulation Mortar (RTIM), which combines the TRM technique with a thermal insulation mortar. The retrofitting techniques herein studied were detailed and designed for envelopes of existing RC buildings.

Nonetheless, as can be seen above, no reference specimen was considered in this testing campaign. The results of the specimens tested in this study will be compared with the specimen Inf_08 tested by Furtado et al. [23]. This specimen has the same geometry, materials and labour as those studied here. The main difference is that the wall was not retrofitted and has only plaster on its external surface. Details concerning the material and mechanical properties of this specimen, herein designated as "REF", can be found in Ref. [20]. The OOP test result will be presented in subsection 3.6.

2.2. Geometry and construction process

The geometric dimensions of each masonry infill wall are 4.2 m in length and 2.30 in height. All the infill panels have equal geometry with the above-mentioned in-elevation dimensions, made of hollow clay horizontal brick units with 150 mm thickness, as shown in Fig. 1a. No reinforcement was used to connect the infill panel and the surrounding RC frame since it represents a common construction practice in Southern European Countries. Also, no gaps were used between the panels and the frame elements and no openings. The walls were built aligned with the outer side of the RC beam, as shown in Fig. 1b.

Each masonry infill wall was built inside an RC frame, composed of RC columns with a cross-section of 300 × 300mm^2 and a longitudinal reinforcement consisting of 4φ16+2φ12. The transversal reinforcement is φ8mm//50 mm along the plastic hinge length (500 mm) and φ8mm//150 mm between the plastic hinges. The RC beams have a cross-section of 500 × 300mm^2 and a longitudinal reinforcement consisting of 5φ16+5φ16. The transversal reinforcement is φ8mm//100 mm along the plastic hinge length (500 mm) and φ8mm//200 mm between the plastic hinges. The RC frame was designed according to Eurocode 8 for a medium ductility class.

2.3. Description of the retrofitting techniques

Specimen E was retrofitted with the traditional ETICS in the exterior surface of the wall. The ETICS was applied over the plaster (10 mm layer; M5 mortar), as shown in Fig. 2a. Expanded polystyrene (EPS) plates 60 mm thick, made of graphite additives with thermal conductivity of 0.031 W/(m.K), were positioned and fixed using an adhesive mortar. In addition, the EPS plates were positioned using plastic connectors to connect them to the wall and the RC frame, as shown in Fig. 2b. The number of connectors was defined according to the supplier's recommendations, namely, four plastic connectors per square meter were adopted per square meter. The plastic connectors were used in both panel and RC frame elements. After that, a new thin layer of adhesive mortar (around 0.5~1 mm) was applied to fix a nonstructural mesh used to prevent cracking due to temperature variations, as shown in Fig. 2c. Finally, the retrofitting was concluded with the application of other 1 cm plaster.

The specimen S was retrofitted with TRM, using a glass-fiber reinforced mesh with a tensile strength equal to 40 kN/m, an ultimate

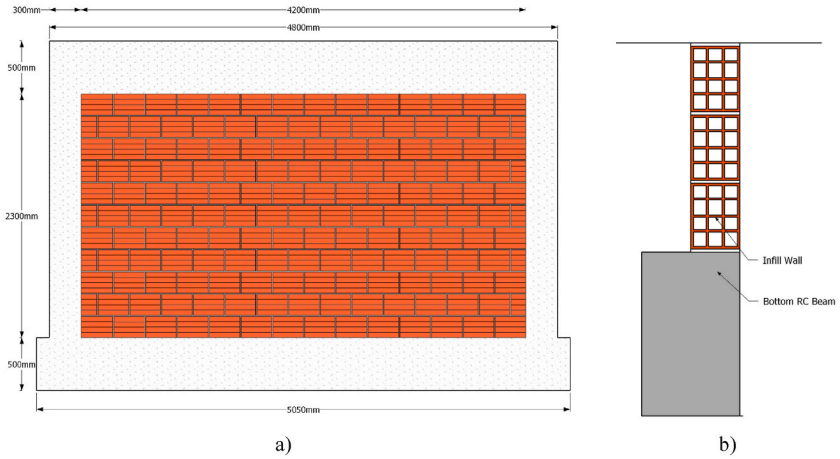

Fig. 1. Infilled RC frame specimen dimensions (units in millimetres): a) geometric dimensions; b) construction detail of the masonry infill walls.

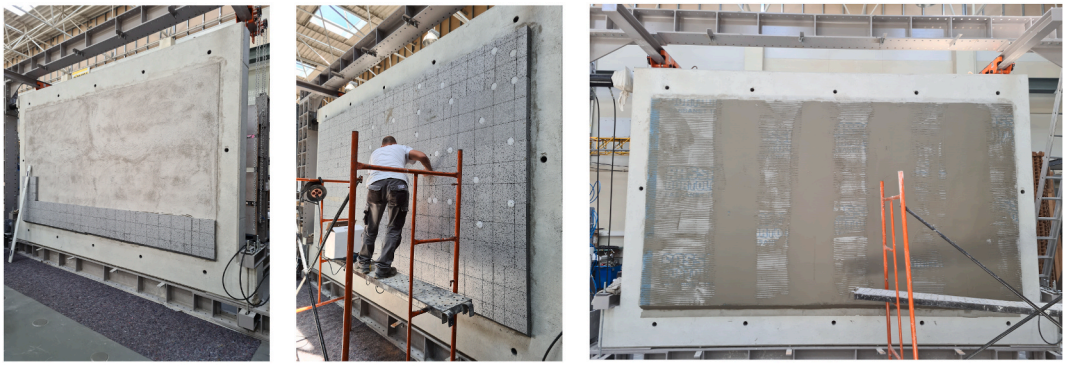

Fig. 2. Retrofitting process of specimen E: a) positioning of the EPS plates; b) application of the plastic connectors; and c) application of the nonstructural mesh.

strain of 3.4% and a grid equal to 16.7 × 16.7 mm^2. The application procedure of this strengthening strategy started with the application of 15 mm layer of a fiber-reinforced plaster. The plaster was sprayed according to the construction practice suggested by the supplier to ensure a better bonding between the mortar and the wall surface and the textile mesh. Five vertical strips (1000 mm width) were used to strengthen the wall overlapped to each other. The application of vertical strips resulted in easier with respect to the application of horizontal strips (whose length can also be very different depending on the bay length). The overlap length used between each vertical strip was 10 cm. The mesh was extended for 15 cm both on the beams and columns. Then, in the overlapping regions for the transition RC frame-infill panel, a duplicated mesh was assumed with an overlap equal to 30 cm (15 cm for the RC frame and 15 cm for the infill panel). After that, helicoidal steel connectors were used to fix the reinforcing mesh to the RC elements (Fig. 3). The length of each connector was 500 mm and they were only applied in the interface between the frame elements and the wall. The distance between connector was defined to be 500 mm. First, the hole was drilled for each connector and then pushed in the hole with a hammer-vibration-based equipment. The impact of the equipment in the connector ensured that the connector was well fixed. After that, the connector was folded and directed to the wall interior until it touched the mesh. The retrofitting process finished with applying a layer of 20 mm of fiber-reinforced plaster.

The retrofitting of the specimen SpE_1 started by fixing the EPS plate (same used in specimen E), using an adhesive layer, with a

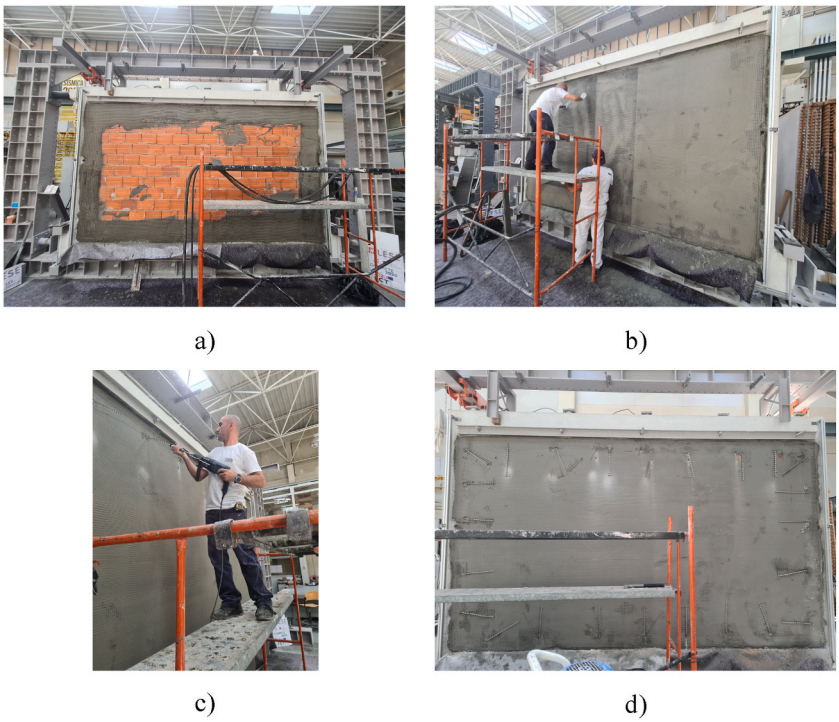

Fig. 3. Retrofitting process of specimen S: a) application of the first layer of mortar; b) application of the reinforcing mesh; c) connectors application; and d) overview of the position of the connector.

150 mm overlap to the RC frame elements in mismatched rows. After that, it was applied over the external surface of the EPS plate, a new layer of adhesive mortar (~5 mm). The GFRP mesh applied in the wall S was applied in the front of the EPS layer, using the same layout (i.e. overlapping frame-wall, between mesh stripes) as shown in Fig. 4. Then, several connectors were used to fix the reinforcing mesh to the wall and RC frame elements. The connectors used are made of plastic bushing with steel screw, as shown in Fig. 4f. The adopted distance between connectors 500 mm in both horizontal and vertical alignments. After that, a new layer of adhesive plaster was applied to the wall surface to receive the nonstructural mesh to prevent cracking. The retrofitting was concluded with the application of ~10 mm adhesive plaster.

A different approach was adopted for the retrofitting process of the specimen ES_2. In particular, the major differences are the use of fiber-reinforced mortar, the type of connectors, and the position of the reinforcing textile mesh. The retrofitting process started with spraying of 10–20 mm of a fiber-reinforced plaster along a 1-m-wide strip so that the reinforcement mesh could be applied with the fresh mortar to achieve better adhesion. Then, the glass-fiber reinforcing mesh (same as the one used in specimen S and ES_1) was placed over the fresh plaster with a 1-m-wide stripe and 150 mm overlapping the RC elements. It was adopted an overlapping between textile meshes of 100 mm. After the application of the fiber-reinforced plaster and textile mesh over the whole panel surface, as shown in Fig. 5, it was performed the application of the connectors to fix the retrofitting material. In this specimen, the connector used was the steel helicoidal one used in specimen S. Similarly to what was performed in the specimen S, the connectors were only applied along the interface between the panel and the RC frame elements. This application required a previous drilling of the RC frame with a diameter of 8 mm and then each connector was applied by punching. These were distributed 500 mm apart and then bent until they were flush against the wall face, and these were applied along the entire perimeter of the masonry wall. After this step, the reinforcement proceeded with the application of another layer of fiber-reinforced mortar with the same thickness as the previous layer, followed by the application of the EPS plates using an adhesive mortar. Then, plastic connectors (4 per m^2) were applied over all the EPS plates to fix them to the wall and frame elements. Finally, the nonstructural mesh was applied using a thin layer of adhesive mortar (~0.5 mm).

The specimen ES_3 was retrofitted with RTIM. The retrofitting process started with the application of a first layer of plaster (~10 mm) to increase the bonding properties, as shown in Fig. 6a. After that, it was applied a glass-fibre mesh with a tensile strength of 921 MPa and a matrix equal to 30 × 40mm^2, as shown in Fig. 6b. The connectors were placed to fix the mesh to the wall and RC elements. The connectors used in this specimen were made of the plastic bushing with plastic bushing with steel screws (same as the ones used in ES_1). The distance between connectors were 500 mm in length and 500 mm in height, as shown in Fig. 6c and d. Therefore, it was sprayed the thermal insulation plaster over the whole panel and frame elements with a total thickness of ~70 mm (Fig. 6e). After the spraying it was placed the nonstructural mesh and then a last layer of 5–10 mm of plaster to finish the retrofitting system (Fig. 6f).

2.4. Material properties

Material characterization tests were performed to collect information about the properties of the RC frame (concrete and steel samples), masonry units, masonry walls, plaster and retrofitting material. During the RC frame construction, six cylindrical samples were collected to perform compressive strength tests. From the tests, it was found an average cubic compressive strength ($f_{cm,cyl}$) equal

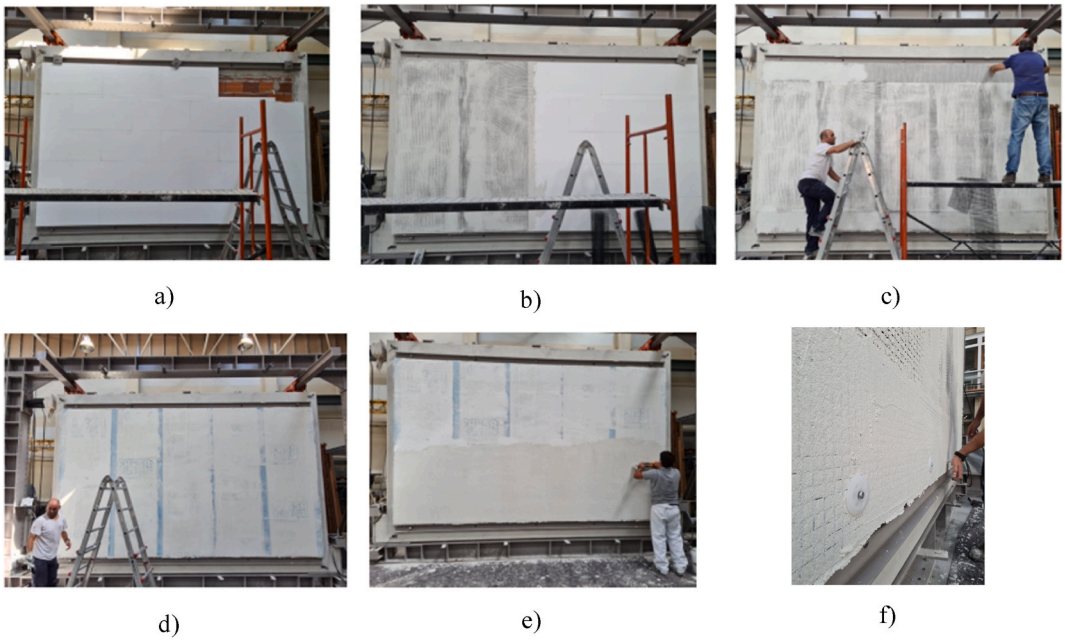

Fig. 4. Retrofitting process of specimen ES_1: a) positioning of the EPS plates; b) application of the reinforcing mesh (vertical strips) and c) horizontal strips in the top and bottom interfaces; d) application of nonstructural mesh; e) application of last layer of adhesive mortar; f) detail of the connectors used to fix the retrofitting material to the RC frame.

Fig. 5. Retrofitting process of specimen ES_2: a) application of a first layer of mortar; b) connectors application; c) Connectors positioning process; d) application of EPS plates; e) application of nonstructural mesh; and f) profile view of the retrofitting layers.

to 22.85 MPa with a standard deviation (SD) of 0.88 MPa and a coefficient of variation (CoV) of 6.1%. The concrete average elastic modulus obtained was 24.3 GPa with an SD of 0.21 GPa and a CoV equal to 0.9%. Also, three samples of each longitudinal reinforcement bar diameter and transverse reinforcement were collected and tested according to the EN10002-1 [24]. From the test results, the yield strength and young modulus of the steel bars are 535 MPa and 198 GPa for the φ8mm bars, 526 MPa and 192 GPa for the φ12 mm bars and 532 MPa and 187 GPa concerning the φ16 mm bars, respectively.

Hollow clay horizontal brick units with 200 mm in-height, 300 mm in-length and 150 mm thick were used to build the masonry infill walls. The percentage of voids is in average around 73%. Compressive strength tests along the direction perpendicular to the horizontal holes were carried out on the masonry units according to EN 771-1. It was found an average value of 1.04 MPa, a CoV equal to 23.6% and a SD of 0.24 MPa. Compression strength tests perpendicular to the horizontal bed joints were carried out in masonry walls, according to EN 1052-1 [25], where the masonry compressive strength and elastic modulus were determined. Diagonal tensile strength tests were performed according to RILEM TC-76-LUM [26], from which it was determined the diagonal tensile strength and shear straining. Finally, flexural strength tests parallel and perpendicular to the horizontal bed-joints were carried out according to EN 1052-2 [27]. The summary of the mechanical properties is presented in Table 1.

From the results, the masonry compressive strength is about 60% higher than the diagonal tensile strength. Also, the flexural strength perpendicular is 36% higher than the parallel to the horizontal bed-joints. The elastic modulus is 98% higher than the shear straining.

Additionally, flexural and compression strength mortar tests were carried out in mortar specimens, according to EN 196–2006 [28]. Six samples, $40 \times 40 \times 160 mm^3$ were tested for each infill panel build (both mortar used to build the panel and mortar used for strengthening). The results from tests performed in mortar specimens collected during the construction of the walls are summarized in Table 2. The results show that the compressive strength is around 6.60 MPa, except for ES_2 where it was obtained 8.23 MPa. This value may be justified due to slight variations in the water content during the mortar preparation. Regarding flexural strength, the results obtained ranged between 1.99 MPa and 2.75 MPa. The adhesive plaster used in specimens E, ES_1 and ES_2 has a compressive strength equal to 18.77 MPa (CoV: 1.70%) and a tensile strength of 5.60 MPa (CoV: 6.90%). The specimens S and ES_2 were retrofitted with a fiber-reinforced plaster with a compressive strength equal to 18.84 MPa (CoV: 1.70 MPa) and a tensile strength of 5.60 MPa (CoV: 6.90%). Finally, the thermal insulation plaster used in the specimen ES_3 has a compressive strength of 0.32 MPa (CoV: 4.1%) and a tensile strength of 0.26 MPa (CoV: 1.5%).

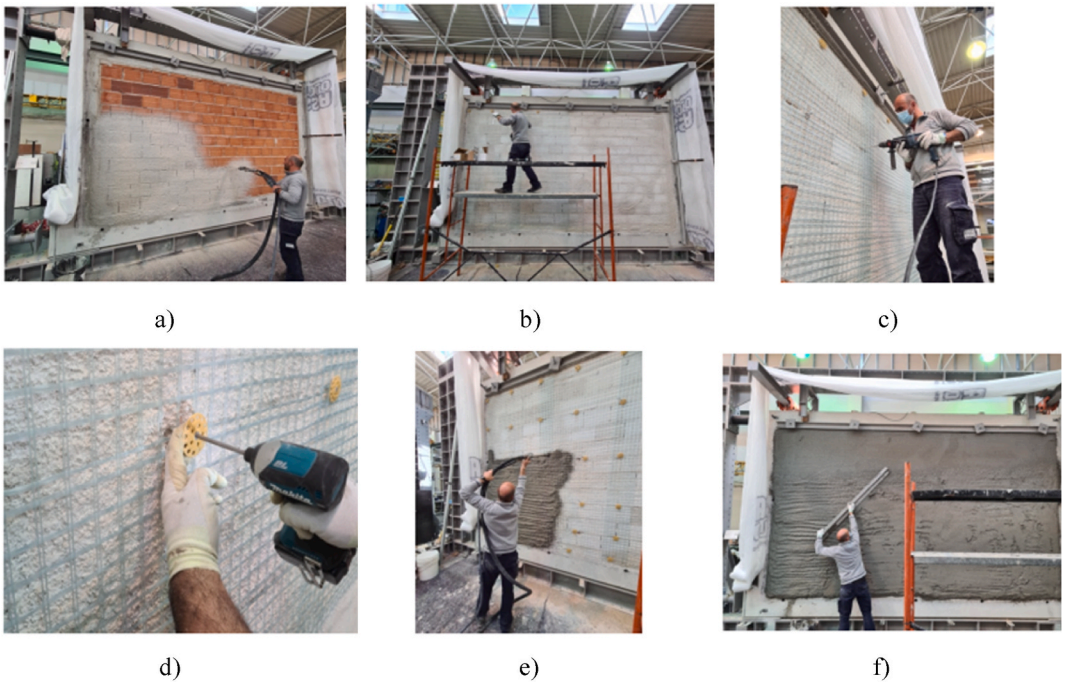

Fig. 6. Retrofitting process of specimen ES_3: a) application of the first layer of plaster; b) application of the textile mesh; c) application of the connectors; d) detail of the connector application; e) spray of the thermal insulation mortar; and e) finalization of the last layer of the thermal insulation plaster.

Table 1
Summary of material properties.

Material	Material properties	Average value (MPa)	CoV (%)	SD (MPa)
Concrete	Compressive strength	22.85	6.1	0.88
	Elastic modulus	24 300	0.9	210
Steel rebars	Elastic Modulus			
	Φ8mm	198 000	5.4	10 692
	φ12mm	192 000	6.2	11 904
	φ16mm	187 000	2.1	3927
	Yielding strength			
	Φ8mm	535	2.2	11.8
	φ12mm	526	3.5	18.4
	φ16mm	532	3.2	17.1
Masonry units	Compressive strength	1.04	23.6	0.24
Masonry walls	Masonry walls compressive strength perpendicular to the horizontal holes	1.09	12.8	0.14
	Elastic modulus perpendicular to the horizontal holes	1975	36.7	719
	Diagonal tensile strength	0.65	22.2	0.14
	Shear straining	996	8.9	88.7
	Flexural strength parallel to the bed-joints	0.22	17.6	0.04
	Flexural strength perpendicular to the bed-joints	0.30	7.90	0.02

Table 2
Results from flexure and compressive strength tests on mortar specimens.

Specimen	Mortar used in the wall construction		Mortar used for plastering	
	Flexure strength (MPa)	Compressive strength (MPa)	Flexure strength (MPa)	Compressive strength (MPa)
E	2.11 (CoV: 0.90%)	6.60 (CoV: 0.60%)	2.17 (CoV: 6.80%)	6.20 (CoV: 2.80%)
S	2.29 (CoV: 4.30%)	6.40 (CoV: 5.80%)	N/A	N/A
ES_1	2.14 (CoV: 9.20%)	6.07 (CoV: 3.50%)	2.65 (CoV: 0.10%)	5.10 (CoV: 5.40%)
ES_2	2.75 (CoV: 10.20%)	8.23 (CoV: 5.90%)	N/A	N/A
ES_3	1.99 (CoV: 6.20%)	6.61 (CoV: 3.70%)	N/A	N/A

2.5. Description of the test setup and instrumentation

Each quasi-static OOP test consisted of applying a distributed OOP loading through twenty-eight pneumatic actuators that mobilized the entire infill panel surface. One wood plate (500 × 500mm^2) per actuator was placed in the front of the, as shown in Fig. 7. Between the infill wall's surface and the wood panel, a 7 mm thick cork plate was included to help distribute the load avoiding possible stress concentration and local failures. The pneumatic actuators are linked to a steel reaction structure. This steel reaction structure comprises four horizontal steel elements (HEB200), which react against five vertical steel elements (HEB 220). The horizontal steel elements are coupled with hinged devices that allow lateral sliding.

The steel reaction structure is attached to the RC frame in twelve different points (5 in the bottom beam, 5 in the top beam, and 2 in middle-height columns) through steel bars φ16mm that are coupled with load cells to allow monitoring the OOP loadings. The number of anchorages were defined based on the numerical simulations that were developed to ensure a low distributed stress along the RC elements, avoiding excessive deflections that may affect the masonry infill walls OOP behaviour. The main objective was to create a self-equilibrated system that balances the transmission of the OOP loadings to the reaction frame.

One of the advantages of this test setup is the possibility of placing the instrumentation in the backside of the reaction structure, allowing performing OOP tests until the panel collapse without damaging any equipment.

It is important to stress that different types of experimental approaches can be used to simulate the OOP seismic loadings on the masonry infill walls. Quasi-static, pseudo-dynamic and dynamic loading tests. All of them can simulate and cyclic horizontal load in the out of plane direction, ir order to reproduce the seismic actions and be used to study the seismic response of the infill walls, with advantages and disadvantages in all the approaches. Quasi-static loadings approach allows to characterize with detail the entire cyclic response of the wall when subjected to OOP loadings, not with random loading like an earthquake but with a controlled imposed displacement. Different strategies are used to apply the loadings, i.e. localized loadings (one-point, three-point or four-point) or distributed loadings (e.g. using airbags or pneumatic actuators). The disadvantage associated with the quasi-static loading approach is associated with some mechanisms that can be triggered due to the OOP velocity demands. Nevertheless, the scientific community recognises quasi-static testing as the best approach to perform a complete experimental characterization of structural elements subjected to horizontal loadings, that may help the calibration of numerical models to further study other types of loads. Finally, the characteristics of pseudo-dynamic and dynamic testing (i.e. shake-table tests) are deeply discussed in Ref. [29].

2.6. Instrumentation and loading protocol

The instrumentation used in each test comprised 3 different groups: i) twenty-five Linear Variable Displacement Transducers (LVDT's) were used to measure the panel's OOP displacements along five horizontal and vertical alignments: ii) five LVDT were used to measure the OOP displacement of the RC frame elements; iii) one LVDT was used in the top beam to measure the vertical displacements at mid-span and thus monitor the evolution of possible arching mechanism development. The schematic layout of the instrumentation used for each specimen is shown in Fig. 8.

The loading protocol is based on the protocol used in the previous tests [30] and consists of the application of several half-cyclic OOP displacements (loading-unloading-reloading) that were imposed with steadily increasing displacement levels, targeting the following nominal peak displacements at the control node located in the center of the panel (sensor W13): 0.5, 1, 1.5, 2, 2.5, 3.5; 5; 7.5; 10 mm; and then 5 by 5 mm up to a maximum OOP displacement of 120 mm (largest capacity of the pneumatic actuators). Each test stopped when the wall reached the collapse, except for specimen S and ES_2 where it reached only the partial collapse of the wall. Two half-cycles were repeated for each lateral deformation demand level. No axial load was applied at the top of the adjacent RC columns.

3. Discussion of individual results

3.1. Specimen E

During the test, it was observed first a detachment of the wall from the surrounding RC frame (Fig. 9a), showed a rigid body

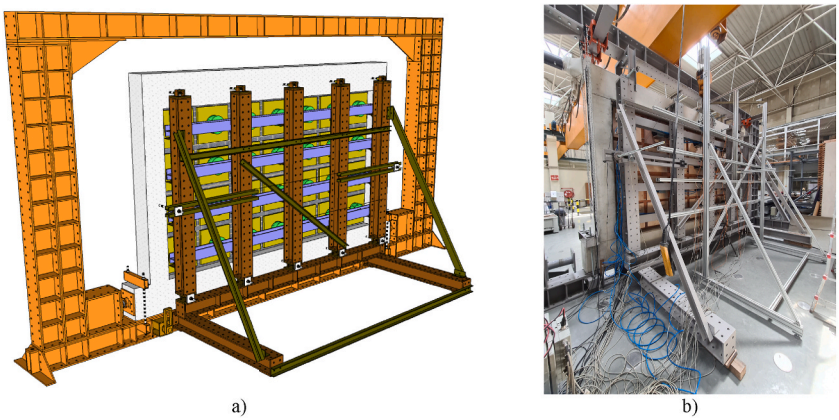

a) b)

Fig. 7. General view of the OOP test setup: a) schematic layout and d) backside view.

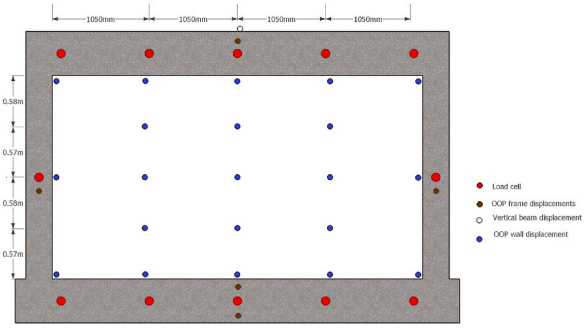

Fig. 8. Instrumentation: schematic front layout.

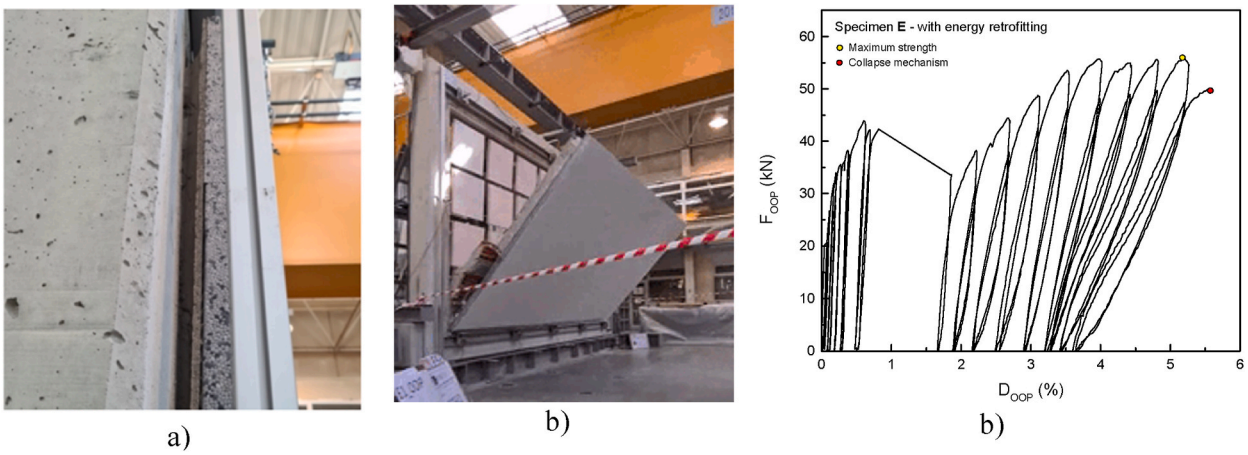

Fig. 9. Specimen E: a) Panel detachment in the top interface; b) Collapse mechanism; and b) Force-displacement curve.

behaviour with the most considerable detachment in the top interface and decreasing up to the bottom. The weakest interface of the wall can justify this is the top one due to the difficulty associated with the construction of the last row of the wall and fulfill of the interface between the wall and the top beam with mortar. Also, the plastic connectors were insufficient to support the stress demands subjected during the test and deformed progressively. The connector deformation led to its expulsion from the RC elements and increased the wall deformation. With the progression of the test, it was observed a larger separation of the wall in the top interface, but no cracking was reported. The absence of cracking is, naturally, due to the presence of the nonstructural mesh that is usually used to prevent cracking development due to temperature variations. Suddenly, it occurred the panel collapsed without the observation of prior significant damage/cracking. It was observed a rigid body behaviour even during the collapse mechanism, as shown in Fig. 9b. After the wall collapse it was not observed the presence of any connector in the RC frame elements, i.e. they were all expulsed during the collapse mechanism (see Fig. 9b).

Concerning the force-displacement curve, shown in Fig. 9c, it was observed an initial stiffness of 24.8 kN/mm. The first detachment occurred for an OOP drift of 0.82%, which caused a slight reduction of the panel strength and shifted the OOP drift to 1.86%. The slight sliding/detachment in the top interface of the masonry infill wall is a common occurrence when the wall is subjected to OOP loading demands, especially for low displacement demands. The cause of the sliding/detachment is related to the construction process of the wall, specifically the way in which the top bed joint between the wall and the top RC beam is performed. During construction, the top bed joint is filled with mortar. However, due to the limited space available for ensuring a perfect filling with mortar, the boundary condition at this interface can be compromised, making it the weakest point in the wall. As a result, when the wall is subjected to OOP loading, the sliding at the top interface occurs as the mortar bed joint is not strong enough to resist the imposed load before developing the arch mechanism. The same was observed in walls S and REF.

After that, the OOP strength increased from 39 kN up to the maximum peak load of 55.9 kN with a corresponding drift of 5.2%. Then, the collapse occurred in the following loading cycle without any previous strength reduction. It can be also observed that the OOP strength capacity in the second loading cycle for the same displacement target is about 17% lower than the one observed in the first loading cycle.

3.2. Specimen S

During the test, several minor cracks (<1 mm) were observed in the first target displacement cycle and the distribution of the

cracking was globally uniform along the entire wall surface. Then, a slight detachment of the wall from the top interface was observed when the peak load was reached. After that, a progression of the cracks and the appearance of new ones was observed until the OOP drift of 3.1% when a main vertical cracking occurred at the panel middle-span (marked in red in Fig. 10a). Then, the wall behaved as a rigid body, the largest OOP displacement observed at the top of the wall and decreasing towards the bottom interface. The ratio between the OOP displacements measured in the top interface and the reference point was around 2 times. Then, the test was interrupted when the drift reached ~6.9%, due to the actuators reached the maximum amplitude in the top horizontal alignment. After the adjustimento of the actuators and the test's restart, the continuous increase of the OOP displacement was observed with a very good efficiency of the connectors preventing the collapse of the wall. As can be observed in Fig. 10b, the level of displacements in the top interface was around 25–30 cm. It was decided to stop the test since the loading system could not impose the wall collapse. Regarding response parameters, the initial stiffness of the wall was 24.36 kN/mm, and the peak load of 100.5 kN was reached for an OOP drift equal to 2.88%. The conventional failure occurred for an OOP drift of 5.23%, and the test stopped (partial collapse stage) for a drift equal to 8.98%. The force-displacement curve is plotted in Fig. 10c.

3.3. Specimen ES_1

Three different damage stages characterized the test of the specimen ES_1. Initially, a progressive increase in deformation was observed in the central zone of the wall, as illustrated in Fig. 11a. After that, the detachment of the wall's lower interface resulted from the plastic connectors rupture. Fig. 11a also shows the bottom zone of the wall, with parts of crushed bricks in the floor caused by the crushing of the bricks near the bottom interface. The deformation between connectors at the bottom interface increased until the failure of each connector. After the failure of all connectors located in the bottom RC beam, the wall deformation increased significantly in this zone. Then, it was possible to observe the failure of the first connector located at mid-span in the upper RC beam (Fig. 11b). After this occurrence, the same phenomenon was verified for the remaining connectors in the upper RC beam. At that moment, the wall was only fixed by the connectrs of the RC columns, which led to an increase of the deformation in the central zone behaving as a panel subjected to unidirectional bending (like a simply supported beam). Finally, the collapse of the wall occurred as a result of the failure of the connectors placed in the RC columns. The panel behaved as a rigid body, as shown in Fig. 11b. The force-displacement curve is presented in Fig. 11c, where it is possible to observe an initial stiffness of 13.66 kN/mm, and a peak load of 81.35 kN for an OOP drift equal to 1.98%. The conventional failure occurred for an OOP drift equal to 3.89%. The collapse occurred for an OOP drift of 11.48% and a corresponding force of 16.54 kN.

3.4. Specimen ES_2

The wall started to detach at the top interface, as illustrated in Fig. 12a, for low displacement demands (~3 mm). This detachment progressively increased until a value of more than 20 mm thick. At this moment, it was possible to register the bricks crushing on the inner face of the wall (i.e., face against the pneumatic actuators). It also triggered the slight detachment of the wall at the bottom interface until the connectors placed in the upper RC beam reached the rupture. After, the wall started to behave as a rigid body supported on the bottom RC beam (similar to what happened in specimen S). This behaviour was due to the remaining connectors placed in the RC elements that prevented the wall collapse up to this stage. After reaching a significant deformation, the partial collapse of the wall occurred, and it was characterized by: i) separation of the wall into two half-span divided bodies; ii) total separation of the wall from the top RC beam (Fig. 12b); and iii) remaining partially supported on the side edges and the bottom RC beam. The high efficiency of the connectors used in this strengthening solution was evident since they ensured the prevention of wall collapse even when the wall reached very high drift values. The total collapse of the wall only occurred after the end of the test and with demolition equipment that allowed the wall to be detached from the RC frame.

Fig. 12c presents the force-displacement curve, in which it is possible to find an initial stiffness of 31.89 kN/mm, and a peak load of 99.17 kN for an OOP drift of 3.19%. After the peak load, the detachment of the wall in the top interface occurred, which caused a reduction of the panel strength. The conventional failure occurred for an OOP drift of 7.48%. As mentioned before, the wall's collapse

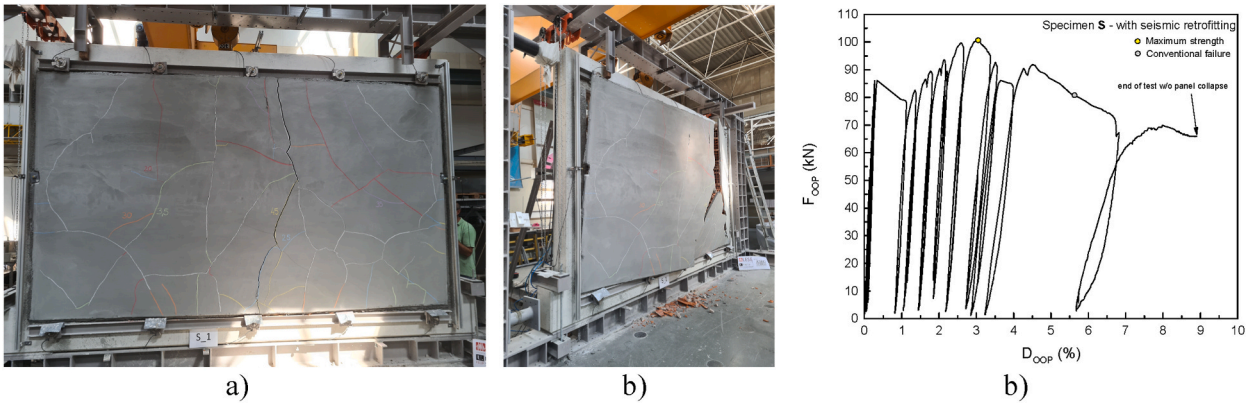

a) b) b)

Fig. 10. Specimen S: a) Global cracking distribution; b) Partial collapse; and b) Force-displacement curve.

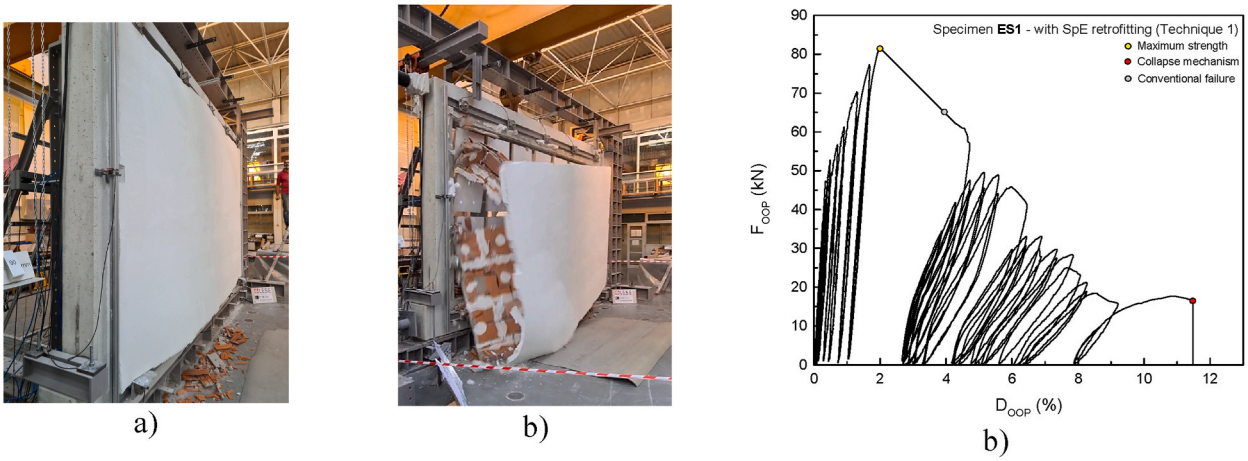

Fig. 11. Specimen ES_1: a) Panel detachment in the bottom interface; b) Collapse mechanism; and b) Force-displacement curve.

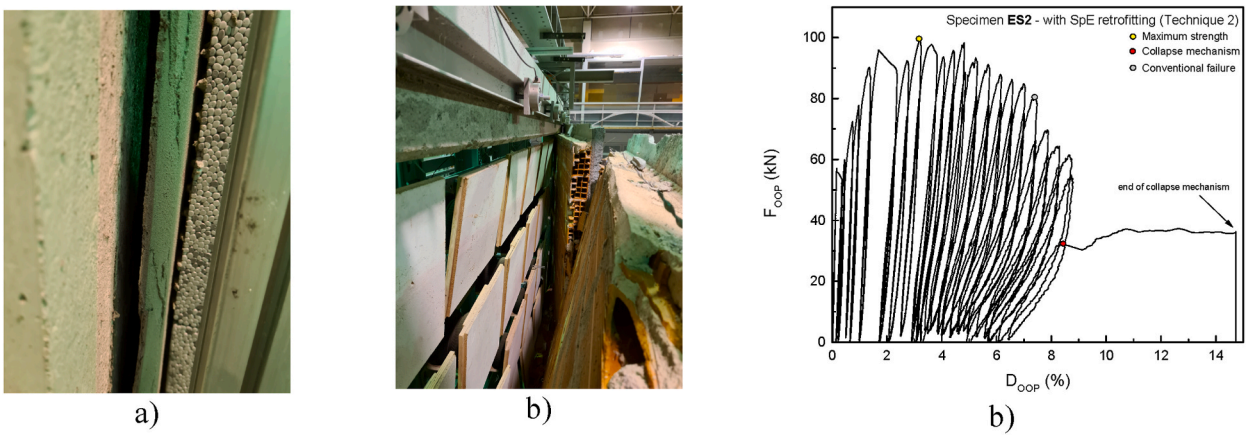

Fig. 12. Specimen ES_2: a) First panel detachment in the left interface; b) Partial collapse mechanism; and b) Force-displacement curve.

did not happen, but the test stopped for an OOP drift of 14.74%.

3.5. *Specimen ES_3*

In the first cycle, a concentration of the OOP deformation in the central region of the wall was observed, as well as the beginning of

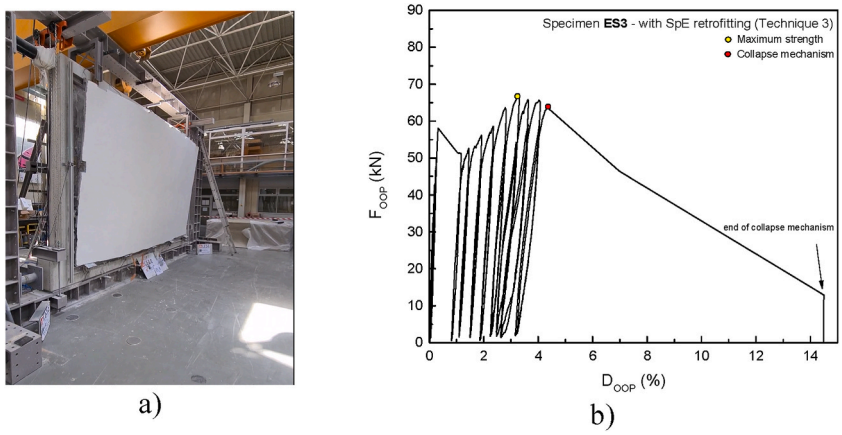

Fig. 13. Specimen ES_3: a) Beginning of the wall collapse mechanism; and b) Force-displacement curve.

cracking in the thermal plaster. This slight cracking was only possible on the left and right sides of the wall since the cracking mesh placed in the external face of the composite retrofitting system prevented the cracks. The low tensile strength of the thermal plaster makes it more susceptible to cracking when compared with other stronger ones (e.g. fiber-reinforced plasters). The cracking developed and increased their thickness until the wall was detached in the top interface. This detachment increased with the test's evolution until the wall's collapse, as presented in Fig. 13a. The collapse occurred without any significant damages visible and without prior strength reduction The collapse of the wall was caused by the fact that the connectors applied at the end (edge) of the reinforcing could not prevent the local failure of the mesh and fixation of the retrofitting composite material. Usually, the filaments at the ends of the mesh are more fragile and can easily break. This is because the frame net has larger grid dimensions than the net used in walls ES_1 and ES_2. This fact contributed to a lower efficiency of the anchorage. Thus, since the mesh broke at the ends around the connectors attached to the RC elements, the wall was left without any element anchoring it to the frame. Thus, the collapse mechanism began once a remarkable detachment occurred at the top interface (see Fig. 13b).

According to the observations, the britle wall collapse for low displacement demands was caused by i) lack of overlapping of the mesh along the interface between the wall and frame elements; ii) the mesh rupture near the connectors placed in the RC frame elements; iii) the large mesh matrix dimensions, which caused high probability of developing very high stresses in the mesh strands when they were contacting the connectors. Risi et al. [31] also reported this type of failure.

From the force-displacement presented in Fig. 13b, an initial stiffness of 18.54 kN/mm and a peak load of 66.91 kN for an OOP drift of 3.16% can be observed. The conventional failure did not occur before the collapse mechanism, which started with an OOP drift of 4.11%.

3.6. REF specimen (without retrofitting)

During the testing of the reference specimen, no damage was observed until reach 5 mm of OOP displacement. At this level of OOP displacement occurred the plaster detachment in some parts of the panel. After that, at the OOP displacement equal to 7.5 mm, the beginning of a horizontal cracking was observed at 1/3 of the panel height. When the panel reached the OOP displacement equal to 15 mm, the horizontal crack became more pronounced and, at the same time, appeared a vertical crack at the middle of the panel, from the top to the horizontal crack. Diagonal cracks were visible when the OOP displacement reached 25 mm, starting in the same horizontal crack alignment until the bottom of the panel. At the end, the panel collapsed at the OOP displacement equal to 30 mm. The cracking pattern was essentially trilinear, as evidenced in Fig. 14a. Fig. 14b presents the force-displacement response curve, from which it is possible to observe that for the OOP displacement equal to 2 mm occurred the first decrease of strength, which was quickly recovered and followed by a progressive increase until the 6 mm (instant where it was visible the beginning of plaster detachment). After that, a progressive increase of the OOP strength can be verified until a maximum peak load equal to 61.2 kN occurs for an OOP displacement equal to 29 mm. After that, at the OOP displacement equal to 29.8 mm, the panel suddenly collapsed without any visible previous decrease in the OOP strength.

4. Global results comparison of the experimental results

This work discusses the effect of retrofitting and the efficiency of the novel SpE retrofitting techniques. Thus, comparing the results obtained by REF wall with those obtained by the retrofitted wall is fundamental. The details of the comparative analysis herein performed are summarized in Table 3. The experimental results described above are compared to each other regarding the response parameters obtained in each OOP force-displacement curve. The comparison between the envelope of all the force-displacement curves is plotted in Fig. 15. The initial stiffness, peak load, ratio between the peak load corresponding drift and ultimate drift, conventional failure corresponding drift and collapse drift are compared and discussed (see Table 4).

The effect of the strengthening on the initial stiffness of the infill walls is unclear since the value obtained by the REF specimen is 33% and % higher than ES_1 and ES_3. The same was not observed in specimen ES_2, which had an initial stiffness 57% higher than the REF wall. In terms of composite SpE retrofitting, their effect on the initial stiffness needs to be deeply studied in the future (e.g. detailed modelling analyses or experimental testing). Concerning the independent retrofitting (i.e. seismic or energy), it was observed that both specimens reached an initial stiffness higher than the non-retrofitting condition. Both retrofitted specimens obtained an initial stiffness

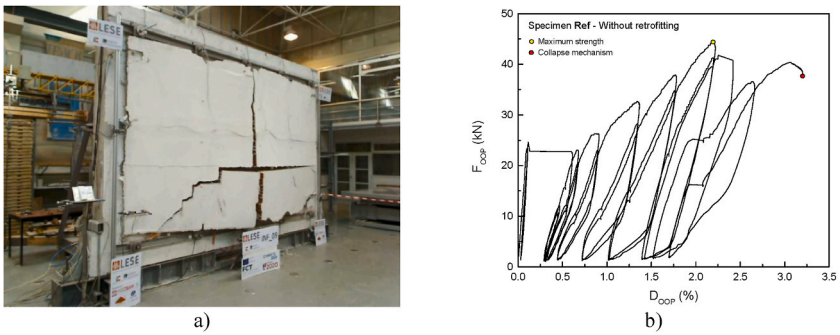

Fig. 14. Specimen Ref: a) Cracking pattern; and b) Force-displacement curve.

Table 3
Summary of the experimental results.

Response parameter	No retrofitting	Energy Retrofitting	Seismic retrofitting	Seismic plus Energy retrofitting		
	REF	E	S	ES_1	ES_2	ES_3
k_{OOPini} (kN/mm)	20.32	24.98	24.36	13.66	31.89	18.54
$F_{OOP,peak}$ (kN)	44.15	55.90	100.5	81.35	99.17	66.91
$d_{OOP,peak}$ (%)	2.21	5.20	2.88	1.98	3.19	3.16
$d_{OOP,conv}$ (%)	N/A	N/A	5.23	3.89	7.48	N/A
$d_{OOP,ult}$ (%)	2.66	5.49	8.98[A]	11.48	14.74 [A]	4.11
$d_{OOP,ult}/d_{OOP,peak}$	1.20	1.06	3.12 [A]	5.80	4.62 [A]	1.30

*Note: N/A: Not applicable since the collapse occurred before reaching the conventional rupture stage; A – This value is related to the drift for which the test was stopped but not referred to the wall collapse.

Table 4
Summary of the thermal conductivity of the materials used in the walls' retrofitting.

Material	Thermal conductivity (W/(m·K))
EPS plate	0.031
Tradional Mortar	1.30
Adhesive mortar	0.60
Fibre-reinforced mortar	0.75
Thermal plaster	0.05

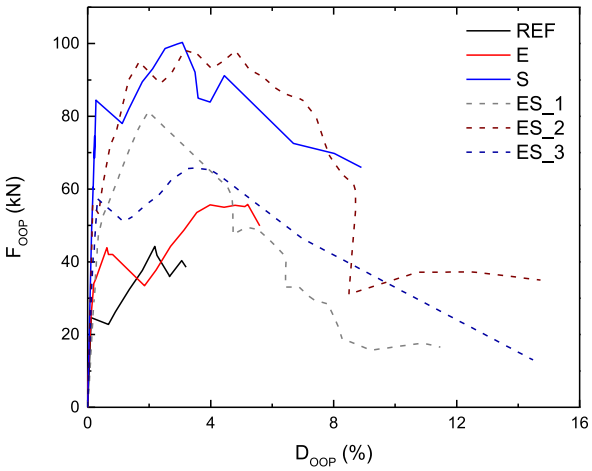

Fig. 15. Global comparison of the force-displacement curves envelopes.

about 20% higher.

The contribution of the retrofitting techniques was significant in the analysis of the maximum peak load. As expected, the maximum strength was reached by wall S but very close to wall ES_2, which is only 1.4% lower. This approximation in strength capacity is justified by the technique used to retrofit ES_2 based on the solution defined for wall S plus the ETIC system. The walls retrofitted with SpE techniques reached a peak load of 52% (ES_3), 84% (ES_1) and 125% (ES_2) higher than the REF specimen. The result obtained by the wall ES_3 is justified by the low efficiency of the anchorage system that did not allow fixing the retrofitting material to the frame elements. Wall E reached a maximum strength 27% higher than REF, which is justified by the contribution of the nonstructural mesh, but it did not achieve a good performance compared with those with SpE retrofitting. For example, it reached 32%, 44% and 17% less than the walls ES_1, ES_2 and ES_3, respectively.

Concerning the comparison between the wall with seismic retrofitting and those with SpE, it must be stated that the maximum strength of the latter was lower, varying between 1.3% and 50%. Regarding the drift for which occurred the peak load, it must be stated that only panel ES_1 reached it for an OOP drift slightly lower than the one observed in the REF (~10%). The remaining walls with SpE retrofitting got the peak load for an OOP drift 40% higher than REF. Wall E was the specimen that reached the peak load for a drift significantly different, namely +135%, than REF.

The conventional failure (i.e. 20% strength drop after the peak load) was reached only in walls S, ES_1 and ES_2. No conclusions can be extracted concerning the level of drift corresponding to the conventional failure since it occurred for low deformation demands for the specimen ES_1 and higher demands for the ES_2. Specimen S is placed between ES_1 and ES_2.

The wall's collapse occurred only in panels REF, E, ES_1 and ES_3. In these tests, it was observed that the highest collapse drift was

the one of ES_1, which was about 332% higher than REF. The reference specimen reached the lowest collapse drift, proving the high vulnerability of the non-retrofitted masonry infill walls. The retrofitting techniques used in walls S and ES_2 were very efficient since they prevented the wall's collapse.

Through the analysis of the ratio between the peak and ultimate drift, it can be stated that the ratio is higher in the walls with SpE retrofitting than the one observed in the REF wall (30–480%). The same was not observed in wall E where the peak load was reached near the instant the wall collapsed.

Finally, some comments should be given on the comparison between the performances of wall E and REF. The main differences between the two walls must be underlined: i) the EPS layer; ii) the non-structural mesh; and iii) the plastic connectors to fix the retrofitting material to the frame elements. The obtained results shouws that the ETIC system slightly modifies the wall bending stiffness which somehow contributes to developing a rigid body behaviour instead of a typical arching mechanism. Also, the plastic connectors are not efficient in preventing the OOP collapse as mentioned before in this report. Based on these points, it may be expected that the ETIC can increase the wall strength capacity, but the deformation capacity is limited by the plastic connectors. However it should be clear that the experimental variability is always an issue, mainly in experimental campaigns with a low number of tests. Additional tests are needed to validate the results herein observed in this study.

5. Combined performance assessment

The performance of RC buildings' envelopes must be analysed by combining the energy and seismic/structural performance. On the one hand, it is well recognized that the envelopes are responsible for a significant part of the energy efficiency of the building. On the other hand, the seismic vulnerability of the envelopes is responsible for multiple fatalities and economic losses.

First, an independent analysis will be performed to check which retrofitting was more efficient. After that, the independent performance assessment will be compared with a holistic performance assessment, where the retrofitting techniques' combined benefit (i.e. energy plus the structural) will be assessed.

The U_{value} was computed for all the walls herein tested using the R_{value} of each layer of the masonry wall (i.e. masonry units, coatings and strengthening material). The U_{value} was computed according to the proposal of EN ISO 6946 [32], given by Equation (1). Each layer's values λ (thermal conductivity coefficient) or Uvalue were necessary for this calculation. In this equation, R_{si} represents the internal surface thermal resistance (value according to EN ISO 6946 [32]), R_{se} represents the external surface thermal resistance (value according to EN ISO 6946 [32]) and R_j is the thermal resistance of the layer of each material.

$$U_{value} = \frac{1}{R_{Si} + \sum_{j}^{j=1} Rj + R_{Se}} \quad \text{Equation 1}$$

Based on the thermal conductivity of each material used for the different techniques (shown in Table, it was found a U_{value} equal to 1.76, 0.39, 1.72, 0.35, 0.30 and 0.37m^2KW^{-1} for the walls REF, E, S, ES_1, ES_2 and ES_3, respectively. The direct comparison between U_{value} of each wall is shown in Fig. 16a. It becomes evident that the walls E, ES_1, ES_2 and ES_3 have a U_{value} much lower than those obtained by REF and S, which is justified by the application of thermal insulation material. Wall ES_2 obtained the lowest U_{value}, about 83% lower than REF and S and about 15% and 19% lower than ES_1 and ES_2.

Concerning the structural performance, two parameters were considered relevant in this analysis: the maximum peak load and the maximum displacement (D_{ult}) reached by each wall. The maximum peak load and displacement obtained by each wall are shown in Fig. 16b and c. The discussion concerning these parameters was already presented in Section 4.

The normalized Uscore was calculated for each wall based on the following assumptions. First, it was determined the range of U_{values} obtained from the walls tested in the experimental campaign. Then, it was assigned a maximum U_{score} of 100 to the minimum U_{value} found within this range (0.3m^2KW^{-1} in our case). This choice reflects the fact that the minimum U_{value} represents the best thermal performance achievable by the tested walls, and it allows for a straightforward comparison of the walls' relative performance. Similarly, it was assigned a minimum normalized U_{score} of 0 to the maximum U_{value} found in the range (1.76m^2KW^{-1} in our case). This choice was made to emphasize the importance of meeting the minimum U_{value} requirements set by energy codes for improving the energy performance of building envelopes.

The same approach was used to compute the normalized structural parameters related to the OOP strength (F_{score}) and displacement (D_{score}) capacity. But in this case, better structural performance is related to the highest F_{OOP} and D_{OOP}, which in this case is 100.5 kN and 14.74% (classified with a score of 100). In the opposite direction, the normalized FOOP and DOOP with the classification of 0 were, as expected, the result of 44.15 kN and 2.66%, respectively. The comparison of the normalized U_{score}, F_{score} and D_{score} is plotted in Fig. 17.

From the analysis of the correlation between the normalized U_{score} and D_{score}, shown in Fig. 17a, it is possible to observe that the wall with better combined performance was the ES_2 with a normalized score of 100 in both parameters. The wall ES_2 also obtained a very interesting score with a normalized U_{score} and D_{score} equal to 96.6 and 73.1. The wall E got a combined performance more better than wall ES_3, mainly because of the very low displacement capacity of the later one. The REF specimen was the one with the worst combined performance, as expected.

Regarding the comparison between U_{score} and F_{score} presented in Fig. 17b, it is worth noting that the wall ES_2 remains the wall with the best overall performance. However, in this case, the F_{score} was 97.6 due to the specimen S reaching the maximum score. The second-best performing wall was ES_1, followed by ES_3. Interestingly, ES_3 showed a significant improvement in both strength capacity and thermal insulation, resulting in a favorable combined U_{score} and F_{score}. Furthermore, wall E exhibited a better combined

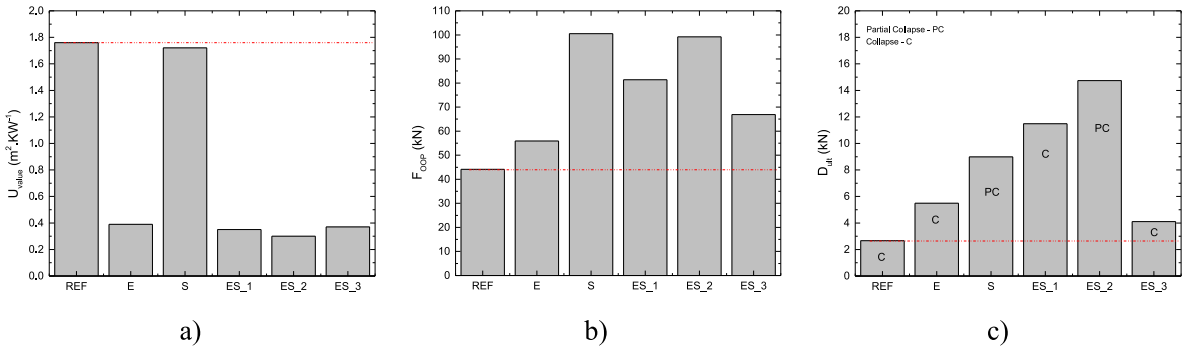

Fig. 16. Independent performance assessment: a) energy efficiency (U_{value}) and b) Structural efficiency (F_{OOP}); and c) Structural efficiency (D_{OOP}).

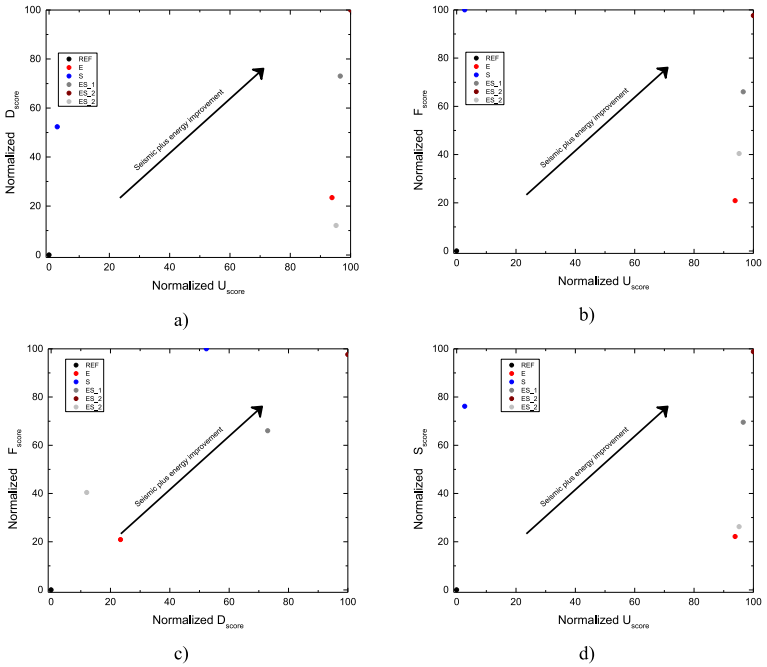

Fig. 17. Combined performance assessment: a) Nomalized D_{score} vs U_{score}; b) Nomalized F_{score} vs U_{score}; c) Nomalized D_{score} vs F_{score} and d) Nomalized U_{score} vs S_{score}.

performance than wall S, primarily due to its low U_{score}. On the other hand, the REF specimen once again had the worst combined U_{score} and F_{score}. Fig. 17c presents a comparison between the two normalized structural parameters. Wall ES_2 showed the best structural performance, mainly due to its high displacement capacity, followed by wall S. It is worth noting that specimen S underwent pure seismic retrofitting, whereas wall ES_2 received a combined retrofitting intervention, highlighting the effectiveness of the proposed technique. Wall ES_1 achieved the third-best performance. The combined structural performance of walls E and ES_3 was similar, with the latter exhibiting lower displacement capacity and the former displaying lower strength capacity.

Finally, a global normalized structural parameter (S_{score}) including both strength and displacement capacities were computed by doing an average of the F_{score} and D_{score}. The comparison between the U_{score} and S_{score} is plotted in Fig. 17d, and it is possible to stress that the better combined performance was achieved by ES_2, followed by ES_1 and ES_3. The wall E got better combined seismic plus energy performance than the specimen S due to the significant impact of the higher U_{score}. Finally, the wall REF was the specimen with poor combined performance.

Another tentative of simplified combined seismic plus energy performance assessment was herein presented by giving a classification between 1 and 6 for each wall for each one of these performance indicators (U_{value}, F_{OOP} and D_{OOP}). Since there are two relevant structural performance parameters instead of the one used for the energy performance it was decided to weight the contribute of each structural parameter by multiplying with a correction factor of 0.5. The classification of 1 point is given for the wall with better performance, i.e. lower U_{value} or maximum F_{OOP} or maximum D_{ult}. In the same way, the classification of 6 points is given for the wall with the worst performance, i.e. higher U_{value} or lower F_{OOP} or lower D_{ult}. From the sum of all the classifications, it was found that the

wall with the best performance was wall ES_2, with a total of 2.5 points. The second was ES_1 with 4.5 points, and the third was wall S with 7 points. The fourth one was wall ES_3 with 7.5 points, followed by wall E with 8.5 points and REF with 12 points. The walls with SpE retrofitting were globally the ones with better-combined performance. It can be observed that the wall ES_1 obtained a score 80% lower than REF, 70% lower than E and 65% lower than the wall S. Concerning the comparison among the walls with combined retrofitting it becomes evident that the ES_2 and ES_1 obtained a very good combined performance and that the poor deformation capacity of wall ES_3 contributed to the poor combined assessment.

Fig. 17 presents the combined assessment that needs to be checked for each infill panel, i.e. the structural (strength and deformation) and energy (Uvalue) input parameters must be analysed simultaneously. The combined SpE improvement equals a simultaneous increase of the structural indicators (strength and deformation) and reduction of the Uvalue. It is clear that, the walls with SpE retrofitting (ES_1, ES_2 and ES_3) achieved a simultaneous SpE improvement. Nonetheless, the combined improvement observed in specimen ES_3 was not so evident compared to ES_1 and ES_2. The independent retrofit (seismic or energy) only allows improving one of the indicators, which means that in seismic-prone regions, the energy retrofitting may not be sufficient to ensure safety. On the other hand, seismic retrofitting may not be enough in zones with severe climates and seismic activity.

It should be stressed that the energy performance assessment herein performed was just a preliminary approach to check if the retrofitting solutions reduced the U-value of the walls to satisfy the thermal energy codes for buildings, where maximum admissible values are proposed for the walls' U-value depending on the climate zone. Of course, this is a basic energy performance assessment and the conclusions herein extracted are based only on the U-value of each wall. The energy performance assessment should be deeply performed through hygrothermal dynamic analyses to compute costs due to energy consumption (e.g. space heating, cooling) and simulate thermal comfort and thus assessing the contribution of each retrofitting technique. For this, it should be used average climate databases.

6. Conclusions and future works

The renovation and refurbishment of existing envelopes of existing RC buildings are usually performed, focusing only on improving their structural or thermal energy characteristics. However, international concern about the sustainability and resilience of existing building structures demands the rethinking of retrofitting techniques that tackle both aspects simultaneously, making the envelopes more energy efficient and seismic safer. Based on this motivation, a testing campaign was carried out to validate the efficiency of novel SpE retrofitting techniques against the independent ones. Five full-scale specimens were built, three of them with SpE retrofitting and two of them with independent. The independent seismic retrofitting technique was a TRM-based technique, and the energy retrofitting was an ETIC system. Two different approaches were assumed for the SpE retrofitting techniques: i) combining TRM and ETIC techniques and varying the disposition of the techniques; ii) reinforcing thermal energy plaster. The five specimens were subjected to pure OOP quasi-static loadings to reach their collapse or partial collapse. Also, the results of the retrofitted walls were compared with a reference specimen (i.e. non-retrofitted) to assess the retrofit benefit better. The following conclusions can be extracted from this research work:

- The SpE retrofitting effect on the initial stiffness of the infill walls is unclear since it was observed, in some cases, a lower initial stiffness of the wall compared with the non-retrofitted configuration. On the other hand, the independent retrofitting increased the initial stiffness about 20% higher;
- The SpE retrofitting was very efficient in increasing the walls' maximum strength, reaching similar values to the one obtained by the wall with pure seismic retrofitting. The SpE retrofitting increased the peak load between 52% and 125%. The independent energy retrofitting increased the peak load by around 27% but reached less than 17–44% than the walls with SpE retrofitting. Concerning the comparison between the wall with seismic retrofitting and those with SpE, it must be stated that the maximum strength of the latter was lower, varying between 1.3% and 50%. Nevertheless, the higher difference was found because of the poor performance of specimen ES_3, which was caused by the poor detailing of the connectors positioned in the RC elements (near the limits of the reinforcing mesh);
- The conventional failure was reached only in walls with seismic or SpE retrofitting. The conventional failure was not observed in the wall without retrofitting and with energy retrofitting since they got a fragile collapse without prior strength reduction;
- Concerning the deformation capacity, it was observed an efficient performance of the SpE retrofitting since the collapse occurred for an OOP drift up to 3.32 times higher. In one case, only partial collapse was reported.

The independent evaluation of the retrofitting efficiency, i.e. seismic or energy, is insufficient for envelopes of buildings located in regions with severe climate and seismically active. If structural safety is the unique parameter studied, the wall with TRM reached the best performance. In the same way, if energy efficiency is only studied, the walls with the ETIC system achieved better performance. On the other hand, if a holistic approach is assumed and both performance indicators are evaluated, the walls with SpE retrofitting get better performance with a particular highlight to the walls retrofitted with the EPS layer combined with application of steel connectors and structural mesh. The effectiveness of retrofitting techniques is a crucial and widely discussed topic in earthquake engineering. Although there are a limited number of investigations on this subject, existing research in the literature has mainly focused on the seismic retrofitting of masonry infill walls. These studies have demonstrated that the connection of the retrofitting material plays a crucial role in the walls' OOP performance. Adequate connection conditions can significantly increase the effectiveness of the retrofitting and prevent the wall from collapsing, whereas inadequate connections, such as those made with plastic connectors, can lead to increased wall collapse vulnerability, as observed by different researchers [13,31,33].

It is reasonable to expect that different types of connectors will result in different outcomes. In the conducted experimental

campaign, it was observed that specimen E, which used plastic connectors to connect the retrofitting material to the frame, had a very low displacement capacity compared to the other retrofitting techniques. Conversely, specimens ES_1 and ES_2, which used different types of steel connectors, exhibited excellent strength and displacement capacity. These findings emphasize the importance of using appropriate retrofitting techniques and connections for effective seismic retrofitting.

It can be observed that the connectors used in the wall ES_1 were effective in contributing to increase the wall displacement (~4x) and strength capacity (~50%), approximately. The connectors were very efficient in accommodating large deformations and dissipating energy along the experimental tests. Nevertheless, the system ES_2 is better because the helicoidal connectors prevent the total collapse of the wall, which in cases of earthquakes with very high pga may play a key difference in terms of life safety. Nevertheless, additional experimental tests and detailed simulations are needed to validate the results herein obtained and to increase and assess the real capacity of connectors used in walls ES_1 and ES_2 under combined in-plane and OOP loadings.

It is important to mention that the thermal plaster used in the wall ES_3 has the capacity of reaching the same energy-saving properties as walls ES_1 and ES_2. The main difference is related to the material cost. The cost of the thermal plaster is significantly higher than the cost of the EPS plates. On the other hand, the time of retrofitting application was much faster in wall ES_3 than in walls ES_1 and ES_2 which can reduce the cost of human resources.

The observations and conclusions herein are related to a limited number of pure OOP tests that need additional validation. Also, the efficiency of the retrofitting techniques needs to be validated when the wall is subjected to combined in-plane and OOP loading demands. Finite element analyses are needed to perform parametric analyses and assess the real impact of the connectors in the RC elements, type of connectors and type of reinforcing mesh. Based on these complementary studies, it will be possible to prepare design guidelines to support the implementation of these techniques in real constructions. Also, a detailed cost-benefit study is necessary to correlate the energy savings with detailed hygrothermal simulations, structural benefits with the results obtained in this testing campaign and the cost of each retrofitting technique.

Author statement

A. Furtado: Conceptualization, Methodology, Formal analysis, Writing - Original Draft, Project administration, Funding acquisition. **H. Rodrigues**: Methodology, Formal analysis, Investigation, Writing - Review & Editing. **A. Arêde**: Methodology, Formal analysis, Investigation, Writing - Review & Editing. **H. Varum**: Methodology, Formal analysis, Investigation, Writing - Review & Editing.

Declaration of competing interest

The authors declare that they have no known competing financial interests or personal relationships that could have appeared to influence the work reported in this paper.

Data availability

Data will be made available on request.

Acknowledgements

The first author is grateful for the Foundation for Science and Technology's support through funding UIDB/04625/2020 from the research unit CERIS. This work was also financially supported by: Project POCI-01-0145-FEDER-007457 - CONSTRUCT - Institute of R&D In Structures and Construction funded by FEDER funds through COMPETE2020 - Programa Operacional Competitividade e Internacionalização and by national funds through FCT - Fundação para a Ci ê ncia e a Tecnologia. This work was also supported by the Foundation for Science and Technology (FCT) - Aveiro Research Centre for Risks and Sustainability in Construction (RISCO), Universidade de Aveiro, Portugal [FCT/UIDB/ECI/04450/2020].

The authors would like to acknowledge Fassa Bortolo for all the materials supplied and technical support that were fundamental for the development of the testing campaign.

The authors would also like to acknowledge the Laboratory of Earthquake and Structural Engineering (LESE) technicians, Mr. Guilherme Nogueira and Mr. Nuno Pinto, for supporting the experimental activity reported in this research work. The authors also acknowledge the constructive comments and suggestions given by the anonymous reviewers which improved the quality of the manuscript.

References

[1] F. Luca, G.M. Verderame, F. Gómez-Martínez, A. Pérez-García, The structural role played by masonry infills on RC building performances after the 2011 Lorca, Spain, earthquake, Bull. Earthq. Eng. 12 (2014//2014), https://doi.org/10.1007/s10518-013-9500-1.

[2] L. Hermanns, A. Fraile, E. Alarcón, R. Álvarez, Performance of buildings with masonry infill walls during the 2011 Lorca earthquake, Bull. Earthq. Eng. 12 (5) (2014) 1977–1997, https://doi.org/10.1007/s10518-013-9499-3.

[3] D. Gautam, H. Rodrigues, K.K. Bhetwal, P. Neupane, Y. Sanada, Common structural and construction deficiencies of Nepalese buildings, Innovative Infrastructure Solutions, journal article 1 (1) (March 29 2016) 1, https://doi.org/10.1007/s41062-016-0001-3.

[4] S. Roeslin, Q.T.M. Ma, H.J. García, Damage assessment on buildings following the 19th september 2017 puebla, Mexico earthquake (in English), Frontiers in Built Environment, Original Research 4 (72) (December-04 2018), https://doi.org/10.3389/fbuil.2018.00072, 2018.

[5] M.T. De Risi, C. Del Gaudio, G.M. Verderame, Evaluation of repair costs for masonry infills in RC buildings from observed damage data: the case-study of the 2009 L'Aquila earthquake, Buildings 9 (5) (2019), https://doi.org/10.3390/buildings9050122. Art no. 122.

[6] C. Del Gaudio, M.T. De Risi, S.A. Scala, G.M. Verderame, Seismic loss estimation in pre-1970 residential RC buildings: the role of infills and services in low–mid-rise case studies (in English), Frontiers in Built Environment, Original Research 6 (188) (November-26 2020), https://doi.org/10.3389/fbuil.2020.589230, 2020.
[7] A. Furtado, H. Rodrigues, A. Arêde, H. Varum, Experimental tests on strengthening strategies for masonry infill walls: a literature review, Construct. Build. Mater. 263 (2020), https://doi.org/10.1016/j.conbuildmat.2020.120520. Art no. 120520.
[8] B. Jelle, Traditional, state-of-the-art and future thermal building insultation materials and solutions-properties, requirements and possibilities, Energy Build. 43 (2011) 2549–2563.
[9] D. Kakaletsis, Comparison of CFRP and alternative seismic retrofitting techniques for bare and infilled RC frames, J. Compos. Construct. 15 (4) (2011) 565–577, https://doi.org/10.1061/(ASCE)CC.1943-5614.0000196.
[10] E. Yuksel, et al., Performance of alternative CFRP retrofitting schemes used in infilled RC frames, Construct. Build. Mater. 24 (2010) 596–609.
[11] A. Dehghani, F. Nateghi, G. Fischer, Engineered cementitious composites for strengthening masonry infilled reinforced concrete frames, Eng. Struct. 105 (2015/12/15/2015) 197–208, https://doi.org/10.1016/j.engstruct.2015.10.013.
[12] K. Kesner, S.L. Billington, Investigation of infill panels made from engineered cementitious composites for seismic strengthening and retrofit, J. Struct. Eng. 131 (11) (2005) 1712–1720, https://doi.org/10.1061/(ASCE)0733-9445(2005)131:11(1712). Article.
[13] L.N. Koutas, D.A. Bournas, Out-of-Plane strengthening of masonry-infilled RC frames with textile-reinforced mortar jackets, J. Compos. Construct. 23 (1) (2019), 04018079, https://doi.org/10.1061/(ASCE)CC.1943-5614.0000911.
[14] F.A. Kariou, S.P. Triantafyllou, D.A. Bournas, L.N. Koutas, Out-of-plane response of masonry walls strengthened using textile-mortar system, Construct. Build. Mater. 165 (2018/03/20/2018) 769–781, https://doi.org/10.1016/j.conbuildmat.2018.01.026.
[15] A. Furtado, H. Rodrigues, A. Arêde, J. Melo, H. Varum, The use of textile-reinforced mortar as a strengthening technique for the infill walls out-of-plane behaviour, Compos. Struct. 255 (2021/01/01/2021), 113029, https://doi.org/10.1016/j.compstruct.2020.113029.
[16] E. Barreira, V.P. de Freitas, External thermal insulation composite systems: critical parameters for surface hygrothermal behaviour, Adv. Mater. Sci. Eng. (2014), 650752, https://doi.org/10.1155/2014/650752, 2014/02/05 2014.
[17] J. Michalak, External thermal insulation composite systems (ETICS) from industry and academia perspective, Sustainability 13 (24) (2021), 13705 [Online]. Available: https://www.mdpi.com/2071-1050/13/24/13705.
[18] G.C. Manos, L. Melidis, K. Katakalos, L. Kotoulas, A. Anastasiadis, C. Chatziastrou, Out-of-Plane flexure of masonry panels with external thermal insulation, Buildings 11 (8) (2021) 335 [Online]. Available: https://www.mdpi.com/2075-5309/11/8/335.
[19] G.C. Manos, L. Melidis, K. Katakalos, L. Kotoulas, A. Anastasiadis, C. Chatziastrou, Masonry panels with external thermal insulation subjected to in-plane diagonal compression, Case Stud. Constr. Mater. 14 (2021), e00538, https://doi.org/10.1016/j.cscm.2021.e00538, 2021/06/01/.
[20] D.A. Bournas, Concurrent seismic and energy retrofitting of RC and masonry building envelopes using inorganic textile-based composites combined with insulation materials: a new concept, Compos. B Eng. 148 (2018/09/01/2018) 166–179, https://doi.org/10.1016/j.compositesb.2018.04.002.
[21] K. Karlos, A. Tsantilis, T. Triantafillou, Integrated seismic and energy retrofitting system for masonry walls using textile-reinforced mortars combined with thermal insulation: experimental, analytical, and numerical study, Journal of Composites Science 4 (4) (2020) 189 [Online]. Available: https://www.mdpi.com/2504-477X/4/4/189.
[22] P.D. Gkournelos, T.C. Triantafillou, D.A. Bournas, Integrated structural and energy retrofitting of masonry walls: effect of in-plane damage on the out-of-plane response, J. Compos. Construct. 24 (5) (2020), 04020049, https://doi.org/10.1061/(ASCE)CC.1943-5614.0001066.
[23] A. Furtado, H. Rodrigues, A. Arede, H. Varum, Experimental investigation on the possible effect of previous damage, workmanship and test setup on the out-of-plane behaviour of masonry infill walls, J. Earthq. Eng. 26 (11) (2022/08/18 2022) 5647–5678, https://doi.org/10.1080/13632469.2021.1882359.
[24] CEN, NP EN10002-1 - Tensile Testing of Mettalic Materials - Part 1: Method of Test at Ambient Temperature, European Committee for Standardization, 2006.
[25] CEN, EN 1052-1 Methods of Test for Masonry - Part 1: Determination of Compressive Strength, 1998.
[26] RILEM, RILEM TC 76-LUM. Diagonal Tensile Strength of Small Walls Specimens, RILEM Publications SARL, 1994.
[27] CEN, EN 1052-2: Methods of Test for Masonry, Determination of flexural strength, 1999.
[28] CEN, EN 196-2006 Methods of Testing Cement, European Committee for Standardization), 2006.
[29] A. Furtado, A. Arêde, J. Melo, H. Rodrigues, N. Pinto, H. Varum, Perspectives and approaches for the out-of-plane testing of masonry infill walls, Exp. Tech. 45 (4) (2021/08/01 2021) 457–469, https://doi.org/10.1007/s40799-020-00413-5.
[30] A. Furtado, H. Rodrigues, A. Arede, H. Varum, Experimental investigation on the possible effect of previous damage, workmanship and test setup on the out-of-plane behaviour of masonry infill walls, J. Earthq. Eng. (2021) 1–32, https://doi.org/10.1080/13632469.2021.1882359.
[31] M.T. De Risi, et al., Influence of textile reinforced mortars strengthening on the in-plane/out-of-plane response of masonry infill walls in RC frames, Eng. Struct. 254 (2022/03/01/2022), 113887, https://doi.org/10.1016/j.engstruct.2022.113887.
[32] ISO, ISO 6946:2017, Building Components and Building Elements — Thermal Resistance and Thermal Transmittance — Calculation Methods, 2017.
[33] M.R. Valluzzi, F. da Porto, E. Garbin, M. Panizza, Out-of-plane behaviour of infill masonry panels strengthened with composite materials, Mater. Struct. 47 (12) (2014/12/01 2014) 2131–2145, https://doi.org/10.1617/s11527-014-0384-6.